Characterization of the Heparin Binding Site in the N-Terminus of Human Pro-Islet Amyloid Polypeptide: Implications for Amyloid Formation†

Andisheh Abedini,‡,§ Sylvia M. Tracz,‡,§ Jae-Hyun Cho,|| and Daniel P. Raleigh*,§,||,⊥

Department of Chemistry, Graduate Program in Biochemistry and Structural Biology, and Graduate Program in Biophysics, State University of New York at Stony Brook, Stony Brook, New York 11794

Received June 8, 2005; Revised Manuscript Received May 5, 2006

ABSTRACT: Islet amyloid deposits are a characteristic pathological hallmark of type 2 diabetes mellitus. Islet amyloid polypeptide (IAPP), also referred to as amylin, aggregates in the islet extracellular space to form amyloid deposits in up to 95% of patients with the disease. IAPP is stored with insulin in β-islet cells and is processed in parallel by subtilisin-like prohormone convertases prior to secretion. There is indirect evidence that normal processing of the prohormone precursor, proIAPP, at the N-terminal cleavage site is defective in type 2 diabetes and results in secretion of an N-terminal extended proIAPP intermediate. The N-terminal flanking region of proIAPP is detected in amyloid deposits; however, the C-terminal flanking region is not. Immunohistochemical studies implicate the presence of the heparan sulfate proteoglycan (HSPG) perlecan in islet amyloid deposits, suggesting a role for HSPGs in mediating amyloid deposition in type 2 diabetes and implicating a binding domain in the N-terminus of proIAPP. Initial studies of proIAPP indicated that the HSPG binding region is contained within the first 30 residues. Here, we characterize the potential HSPG binding site of proIAPP in detail by analyzing a set of peptide fragments. Binding is tighter at low pH due to protonation of histidine residues. Deletion studies show that Arg-22 and His-29 play a role in binding. Reduction of the Cys-13 to Cys-18 disulfide leads to a noticeable decrease in binding. We demonstrate the ability of heparan sulfate to induce amyloid formation in N-terminal fragments of proIAPP. The oxidized peptide forms amyloid more rapidly than the reduced variant in the presence of heparan sulfate, but the reduced peptide ultimately forms more extensive amyloid deposits. The potential implications for islet amyloid formation in vivo are discussed.

Type 2 diabetes mellitus, formerly referred to as non-insulin-dependent diabetes mellitus, is a progressive metabolic disease that occurs widely among the elderly and is quickly becoming a worldwide epidemic in children and obese individuals (*1*, *2*). Type 2 diabetes arises from a deficiency in insulin secretion due to loss of β-cell mass, as well as insulin resistance and defects in insulin action. Islet amyloid polypeptide (IAPP)[1] is colocalized with insulin in β-islet cells of the pancreas and cosecreted with insulin in response to various stimuli, predominantly blood glucose levels (*3*−*6*). It is a normally soluble 37-residue polypeptide hormone and although its functions are not clearly understood, it is believed to play a role in suppression of food intake (*7*, *8*), gastric emptying (*8*), and glucose homeostasis (*9*−*11*). In type 2 diabetes, IAPP aggregates in the islet extracellular space to form amyloid deposits in up to 95% of patients with the disease (*12*−*14*). Studies have shown that the extent of amyloid deposition correlates with the severity of the disease in patients, suggesting a relationship between IAPP deposition in the pancreas and the progression of type 2 diabetes (*15*, *16*).

Insulin and IAPP are synthesized by β-cells as their prohormone precursors, proinsulin and proIAPP, respectively (*3*). Prior to cosecretion, both prohormones are processed in parallel by the action of subtilisin-like prohormone conver-

† Supported by NIH Grant GM70941 to D.P.R. A.A. and S.M.T. were supported by GAANN fellowships from the Department of Education.

* Corresponding author. Phone: (631) 632-9547. Fax: (631) 632-7960. E-mail: draleigh@notes.cc.sunysb.edu.

‡ The first two authors contributed equally to this work.

§ Department of Chemistry.

|| Graduate Program in Biochemistry and Structural Biology.

⊥ Graduate Program in Biophysics.

[1] Abbreviations: BSA, bovine serum α-lactoalbumin; CGRP, calcitonin gene-related peptide; CD, circular dichroism spectroscopy; DIPEA, *N*,*N*-diisopropylethylamine; DMF, *N*,*N*-dimethylformamide; Fmoc, 9-fluorenylmethoxycarbonyl; HBTU, *O*-benzotriazol-1-yl-*N*,*N*,*N*′,*N*′-tetramethyluronium hexafluorophosphate; $hIAPP_{12-22}$, peptide corresponding to residues 12−22 of human pro-islet amyloid polypeptide containing a disulfide bridge between cysteine-13 and cysteine-18; HOBT, *N*-hydroxybenzotriazole monohydrate; HPLC, high-performance liquid chromatography; HSPGs, heparan sulfate proteoglycans; IAPP, islet amyloid polypeptide; MALDI-TOF MS, matrix-assisted laser desorption ionization−time of flight mass spectrometry; MES, 2-morpholinoethanesulfonic acid; mS, milliseimens; ox-pro-$IAPP_{1-30}$, oxidized $proIAPP_{1-30}$; ox-$proIAPP_{1-30}$/HSPG, oxidized $proIAPP_{1-30}$ with heparan sulfate; PAL-PEG, 5-(4′-Fmoc-aminomethyl-3′,5-dimethoxyphenyl)valeric acid; PC2, subtilisin-like prohormone convertase enzyme 2; PC(1/3), subtilisin-like prohormone convertase enzyme 1/3; proIAPP, pro-islet amyloid polypeptide; $proIAPP_{1-12}$, peptide corresponding to residues 1−12 of human pro-islet amyloid polypeptide; $proIAPP_{1-22}$, peptide corresponding to residues 1−22 of human pro-islet amyloid polypeptide; $proIAPP_{1-30}$, peptide corresponding to residues 1−30 of human pro-islet amyloid polypeptide; $proIAPP_{12-22}$, peptide corresponding to residues 12−22 of human pro-islet amyloid polypeptide; red-$proIAPP_{1-30}$, reduced $proIAPP_{1-30}$; red-$proIAPP_{1-30}$/HSGP, reduced $proIAPP_{1-30}$ with heparan sulfate; TEM, transmission electron microscopy; TFA, trifluoroacetic acid; v/v, volume to volume.

10.1021/bi0510936 CCC: $33.50
Published on Web 07/12/2006

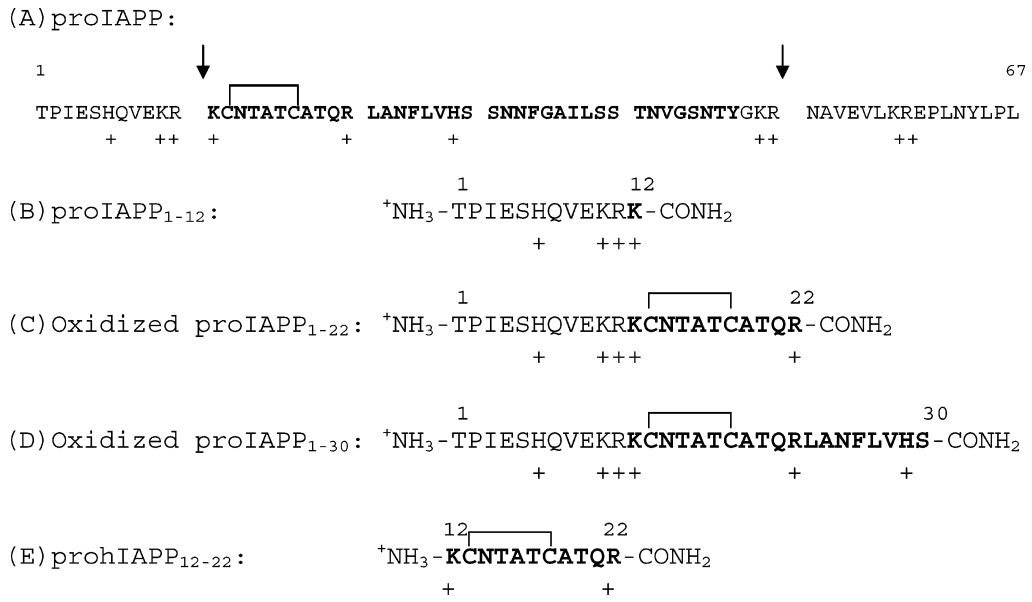

FIGURE 1: (A) Primary sequence of the 67-residue human proIAPP. The mature 37-residue human IAPP is in bold. The naturally occurring protein has a disulfide bridge between Cys-13 and Cys-18 as shown. Positively charged residues are indicated with a + symbol. Cleavage occurs at two dibasic sites indicated by arrows: Lys_{10}-Arg_{11} at the N-terminus and Lys_{50}-Arg_{51} at the C-terminus. The new C-terminus is further processed, resulting in an amidated Tyr at the C-terminus of mature IAPP. Note that the residues in all of the peptides are numbered according to their positions in full-length proIAPP. (B) $ProIAPP_{1-12}$. (C) Oxidized $proIAPP_{1-22}$. (D) Oxidized $proIAPP_{1-30}$. (E) $prohIAPP_{12-22}$. The disulfide bridge between Cys-13 and Cys-18 is depicted by solid lines. All peptides have an amidated C-terminus.

tases PC2 and PC(1/3) within β-cell secretory granules (*17*, *18*). Normal processing of proIAPP, a 67-residue polypeptide, into the mature 37-residue IAPP polypeptide requires cleavage of two flanking fragments at N-terminal and C-terminal sites (*17*). The sequence of proIAPP and the locations of the cleavage sites are indicated in Figure 1. Recent studies have concluded that PC(1/3) is responsible for processing proIAPP at the C-terminal flanking region but not at the N-terminal flanking region (*19*). On the other hand, PC2 can completely process proIAPP to mature IAPP by cleaving at both the N-terminal and C-terminal sites, although cleavage at the C-terminal site is preferred by PC(1/3) (*19*). Loss of or defective processing by PC2 results in secretion of an improperly processed N-terminally extended proIAPP intermediate (*20*, *21*). Immunohistochemical investigation of islet amyloid deposits verifies the presence of the N-terminal flanking region of proIAPP but not the C-terminal flanking region (*22*−*24*). Heparan sulfate, a component of the basement membrane and extracellular matrix of β-cells (*25*), is also present in amyloid deposits, suggesting that it might play an important role in amyloidosis (*22*, *26*). Proteoglycans, particularly perlecan, have been implicated in virtually all human amyloid diseases including Alzheimer's disease, familial amyloidosis, and type 2 diabetes (*25*, *27*−*33*).

HSPGs are ubiquitously expressed on various cell membranes and have been suggested to serve as scaffolds in amyloidosis whereby they stabilize and perhaps induce amyloid formation and protect against proteolysis (*27*, *30*, *31*). The presence of the N-terminal proIAPP flanking region in islet deposits (*22*) suggests that the HSPG binding site is located at the N-terminus of proIAPP. Identification of the binding site in the N-terminus of proIAPP is important since it could aid in the development of new inhibitors of islet amyloidosis.

Heparin, another glycosaminoglycan, has a carbohydrate backbone composition identical to heparan sulfate and is frequently used as a model for tissue heparan sulfates (*34*). Mature IAPP has been shown to bind both heparin and heparan sulfate equally, although this interaction may be due to the peptide's aggressive nature to aggregate (*28*, *35*). Important studies by Park and Verchere demonstrated that a 30-residue peptide corresponding to the N-terminus of proIAPP bound heparin relatively well and that heparin was a valid model for perlecan. Their work also established the importance of a set of basic residues at positions 10, 11, and 12 for binding (*36*). The numbering system used in this work corresponds to that used for proIAPP; thus, Lys-12 is the first residue of the mature hormone. Binding at pH 5.5 was observed to be stronger than at pH 7.4, suggesting a potential role for one or more of the histidines located in the peptides (*36*). Here, we characterize the binding site in the N-terminus of proIAPP in detail and examine the role of His-6, His-29, and Arg-22 in heparin affinity. We also demonstrate an important role for the Cys-13/Cys-18 disulfide bridge in heparin binding and show for the first time that heparan sulfate can induce amyloid formation by fragments that contain the N-terminal pro region of IAPP.

EXPERIMENTAL PROCEDURES

Peptide Synthesis and Purification. Peptides were synthesized on a 0.25 mmol scale using an Applied Biosystems 433A peptide synthesizer, via 9-fluorenylmethoxycarbonyl (Fmoc) chemistry. Solvents used were ACS grade. Reagents were purchased from Advanced Chemtech, PE Biosystems, Sigma, and Fisher Scientific. Use of a PAL-PEG resin afforded an amidated C-terminus. Standard Fmoc reaction cycles were used. The first residue attached to the resin, all β-branched residues, and all residues directly following a β-branched residue were double coupled. The crude peptides were purified via reverse-phase HPLC using a Vydac C18

preparative column. A two-buffer system was utilized. Buffer A consisted of H_2O and 0.045% HCl (v/v). Buffer B consisted of 80% acetonitrile, 20% H_2O, and 0.045% HCl (v/v). All peptides were analyzed by MALDI-TOF MS to confirm their identity.

Peptide Oxidation. Selective intramolecular disulfide bond formation was achieved by air oxidation or by oxidation with DMSO (*37*). For air oxidation, purified reduced peptide was dissolved in 100 μL of 5 M guanidine hydrochloride. The sample was diluted with 200 mM Tris-HCl buffer at pH 8.5 ($\pm$0.3) to give a peptide concentration of 10 μM in 125 mM guanidine hydrochloride. The solution was continuously stirred and exposed to air. For oxidation by DMSO, peptide was dissolved in 100% DMSO and allowed to stand at room temperature for a minimum of 5 h. The reactions were monitored by reverse-phase HPLC using a Vydac C18 semipreparative column. Disulfide formation was confirmed by analysis of the monoisotopic distribution via MALDI-TOF MS.

Heparin-Affinity Chromatography. Low molecular weight heparin−agarose was purchased from Sigma-Aldrich. A 12 mL column of heparin−agarose was equilibrated with the appropriate buffer. Buffers utilized were either 20 mM MES at pH 5.5 ($\pm$0.3) or 20 mM Tris-HCl at pH 7.4 ($\pm$0.3). Approximately 0.5−2.0 mg of peptide was dissolved in 1 mL of buffer and loaded onto the column. The column was washed with 5 column volumes of buffer followed by a 0−1 M NaCl gradient with a flow rate of 1.5 mL/min. The elutant was collected in 5 mL fractions, and the absorbance (at 220 nm) and conductivity (mS/cm) of each fraction were measured and recorded.

Sample Preparation for Biophysical Studies. Biophysical studies utilized peptide samples derived from the same stock solution in order to ensure the same conditions in all experiments. Circular dichroism, transmission electron microscopy, and thioflavin-T binding studies were all conducted using identical conditions. A 6.8 mM peptide solution of oxidized $proIAPP_{1-30}$ was prepared in distilled, deionized H_2O and adjusted to pH 7.4 ($\pm$0.3) using NaOH. Four different solutions were prepared immediately by transferring aliquots of the peptide stock into (1) 20 mM Tris-HCl, (2) a heparan sulfate solution (2 mg/2.2 mL) prepared with 20 mM Tris-HCl, (3) 20 mM Tris-HCl and 3.4 mM DTT, and (4) a heparan sulfate solution (2 mg/2.2 mL) prepared with 20 mM Tris-HCl and 3.4 mM DTT. These solution conditions afforded (1) oxidized $proIAPP_{1-30}$ (ox-$proIAPP_{1-30}$), (2) oxidized $proIAPP_{1-30}$ with heparan sulfate (ox-$proIAPP_{1-30}$/HSPG), (3) reduced $proIAPP_{1-30}$ (red-$proIAPP_{1-30}$), and (4) reduced $proIAPP_{1-30}$ with heparan sulfate (red-$proIAPP_{1-30}$/HSGP) stock solutions, respectively. All four solutions were incubated at room temperature for 89 days and contained 1.4 mM peptide, 53.8 μM heparan sulfate, and 16.6 mM Tris-HCl at pH 7.4 ($\pm$0.3).

Circular Dichroism Spectroscopy. CD experiments were performed using an Aviv Model 62A DS circular dichroism spectrometer. To determine whether the Cys-13 to Cys-18 disulfide bridge has a role in heparan binding and whether heparan binding induces peptide secondary structure, both oxidized and reduced peptide states were monitored in the presence and absence of heparan sulfate. The peptide concentration of the stock solutions is too high to allow CD measurements; thus immediately before the wavelength scans, aliquots of the peptide solutions were diluted into respective buffers, for a final peptide concentration of 70.7 μM in 19.8 mM Tris-HCl and 2.7 μM heparan sulfate at pH 7.4 ($\pm$0.3). Amyloid formation and fibril dissociation are slow for this system; thus the experimental protocol provides an accurate readout of the state of the stock solutions. Far-UV CD experiments were performed using a 0.1 cm quartz cuvette. Wavelength scans were taken at 25 °C with a minimum of five repeats. Spectra were recorded over a range of 190−250 nm at 1 nm intervals with an averaging time of 3 s. Background spectra were subtracted from collected data.

Thioflavin-T Fluorescence. Thioflavin-T binding assays were used to detect the presence of amyloid. Fluorescence emission spectra were measured on a Jobin Yvon Horiba fluorescence spectrophotometer at an excitation wavelength of 450 nm and emission wavelength of 482 nm. The excitation and emission slits were set at 5 and 10 nm, respectively. A 1.0 cm cuvette was used. All thioflavin-T binding experiments were performed by diluting 75 μL of the peptide stock solution (prepared as described above) into Tris-HCl buffers containing thioflavin-T immediately prior to the measurements. Final solution conditions were 19.8 mM Tris-HCl and 25 μM thioflavin-T at pH 7.4 ($\pm$0.3). The total peptide concentration was 70.7 μM in the presence or absence of 2.7 μM heparan sulfate. The solutions were stirred during the fluorescence measurements in order to maintain homogeneity. Note that the fluorescence studies were conducted from the same stock solution that was used for CD measurements. As a control, we also monitored the fluorescence of thioflavin-T in heparan sulfate solutions without peptide. The profiles showed a fluorescence intensity that extended to 472 nm; therefore, we reported our fluorescence measurements at wavelengths greater than 472 nm to reflect only the peptide−dye interactions.

Transmission Electron Microscopy. TEM was performed at the University Microscopy Imaging Center or Life Science Microscopy Center at the State University of New York at Stony Brook. Peptide solutions were incubated at pH 7.4 ($\pm$0.3) as described above. A 4 μL aliquot of the peptide solution was placed on a carbon-coated Formvar 200 mesh copper grid and negatively stained with either saturated uranyl acetate or phophotungstic acid. The TEM experiments used the same stock solutions that were employed for the CD and thioflavin-T fluorescence studies.

RESULTS AND DISCUSSION

Design of Peptides. A set of five peptides derived from the N-terminal region of human proIAPP were synthesized and characterized. The sequences of the peptides are listed in Figure 1. All peptides were prepared with an amidated C-terminus in order to avoid introducing an additional charged group, and the N-terminus was left free. The residues in all of the peptides are numbered according to their positions in full-length proIAPP. The first peptide comprises the first 12 residues of human proIAPP. This peptide contains the entire N-terminal proIAPP flanking region, the first residue of mature IAPP (Lys-12), and is designated $proIAPP_{1-12}$. This peptide was designed to determine if the Lys_{10}-Arg_{11}-Lys_{12} motif is the minimal requirement for heparin binding. The total net charge of this peptide can be varied from +5 at low pH where the Glu's are protonated

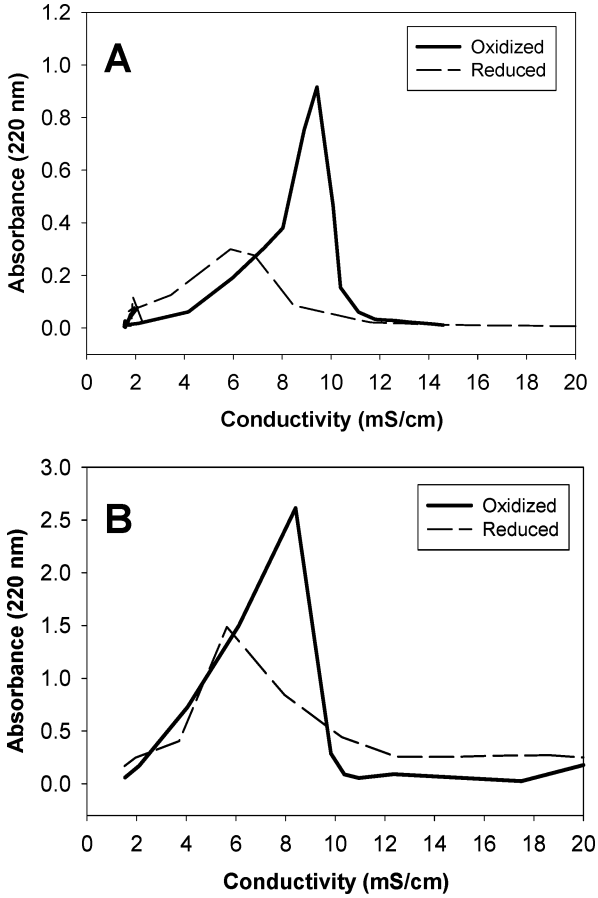

FIGURE 2: Heparin affinity of oxidized and reduced proIAPP$_{1-22}$ and proIAPP$_{1-30}$ at pH 7.4 (±0.3). (A) Elution profile of oxidized and reduced proIAPP$_{1-22}$. (B) Elution profile of oxidized and reduced proIAPP$_{1-30}$. Approximately 0.5−2.0 mg of peptide was dissolved in the appropriate buffer and loaded onto the column. The column was washed with 5 column volumes of 20 mM Tris-HCl at pH 7.4 (±0.3). A 0−1 M NaCl gradient was developed, 5 mL fractions were collected, and absorbance was measured at 220 nm to yield elution profiles. The difference in intensity reflects differences in loading concentration.

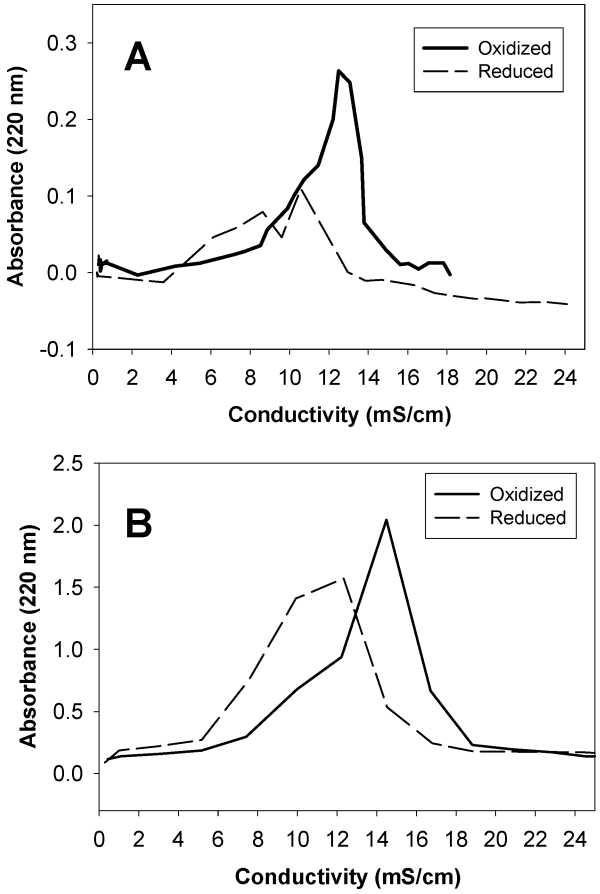

FIGURE 3: Heparin affinity of oxidized and reduced proIAPP$_{1-22}$ and proIAPP$_{1-30}$ at pH 5.5 (±0.3). (A) Elution profile of oxidized and reduced proIAPP$_{1-22}$. (B) Elution profile of oxidized and reduced proIAPP$_{1-30}$. Approximately 0.5−2.0 mg of peptide was dissolved in the appropriate buffer and loaded onto the column. The column was washed with 5 column volumes of 20 mM Tris-HCl at pH 7.4 (±0.3). A 0−1 M NaCl gradient was developed, 5 mL fractions were collected, and absorbance was measured at 220 nm to yield elution profiles. The difference in intensity reflects differences in loading concentration.

to between +1 and +3 at extracellular pH (pH 7.4) depending upon the exact pK_a's of the N-terminus and His-6. The second peptide consists of the first 22 residues of human proIAPP, comprising the entire N-terminal proIAPP flanking region and the first 11 residues of mature human IAPP. It is denoted proIAPP$_{1-22}$. The net charge of this fragment ranges from +4 at the lowest pH studied (5.5) to between +2 and +4 at pH 7.4. The third peptide, designated proIAPP$_{1-30}$, is identical to the 30- residue N-terminal proIAPP fragment initially characterized by Park and Verchere (*36*). The net charge on this fragment will be +5 at the lowest pH studied (5.5) and will be +2 at pHs above the pK_a of both the histidines and N-terminus, but below the pK_a of the lysines. Comparison of proIAPP$_{1-12}$, proIAPP$_{1-22}$, and proIAPP$_{1-30}$ allows us to probe the role of Arg-22 and His-29 in HSPG binding (*36*). ProIAPP contains an intramolecular disulfide between Cys-13 and Cys-18. Consequently, we studied the oxidized and reduced forms of both proIAPP$_{1-22}$ and proIAPP$_{1-30}$ in order to examine the role of the disulfide bridge in heparan binding. The last peptide designed, hIAPP$_{12-22}$, comprises the first 12 residues of mature human IAPP, which are residues 12−22 of proIAPP. The Cys-13 to Cys-18 disulfide bridge is present, and the net charge is +3 when the N-terminus is protonated.

Analysis of Heparin Binding. Heparin-affinity chromatography was used to probe the ability of the various peptides to bind heparin. Elution profiles are reported as absorbance vs conductivity. Bovine serum α-lactoalbumin (BSA) and hen lysozyme were tested as controls for nonspecific heparin binding. BSA is known not to bind to heparin, and both BSA and lysozyme have previously been used as controls in studies of proIAPP fragments (*36*). Both proteins eluted in the void volume. Analyses of the proIAPP$_{1-30}$ and proIAPP$_{1-22}$ fragments directly demonstrate an important role for the disulfide bond. The respective reduced peptides elute at lower conductivity values than their oxidized counterparts at both pH 5.5 (±0.3) and pH 7.4 (±0.3) (Figure 2).

The retention of both fragments by heparin is higher at the lower pH (Figure 3). The pK_a of the N-terminus of these peptides is not known, and it may partially titrate over this range. ProIAPP$_{1-22}$ contains a single His at position 6, and proIAPP$_{1-30}$ contains a second His at residue 29. The pH-dependent affinity is consistent with one or both of these histidines playing a role in the binding interaction. Comparison of the 1−22 fragment at pH 5.5 (±0.3) and 7.4 (±0.3) implicates a role for His-6 and/or the N-terminus. Comparison of the 1−22 fragment to the longer 1−30 fragment at pH 5.5 (±0.3) in turn also implicates a role for

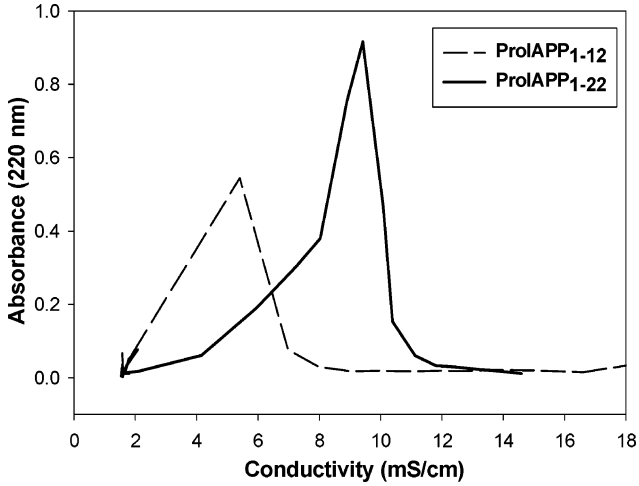

FIGURE 4: Heparin affinity of N-terminal proIAPP fragments. Elution profiles of $proIAPP_{1-12}$ (dashed line) versus oxidized $proIAPP_{1-22}$ (solid line) at pH 7.4 (±0.3). Approximately 0.5−2 mg of peptide was dissolved in the appropriate buffer and loaded onto the column. The column was washed with 5 column volumes of 20 mM Tris-HCl at pH 7.4 (±0.3). A 0−1 M NaCl gradient was developed, 5 mL fractions were collected, and absorbance was measured at 220 nm to yield elution profiles. The difference in intensity reflects differences in loading concentration.

His-29, since the affinity of $proIAPP_{1-30}$ at pH 5.5 (±0.3) is greater than that of $proIAPP_{1-22}$ at pH 5.5 (±0.3). His-29 is the only titratable residue and the only charged residue between positions 23 and 30 and is thus responsible for the tighter binding. Interestingly, there is no significant difference between $proIAPP_{1-30}$ and $proIAPP_{1-22}$ at pH 7.4 (±0.3). Both peptides elute at the same solution conductivity within experimental uncertainty. His-29 is presumably largely deprotonated at this pH, and the results indicate that the tighter binding for $proIAPP_{1-30}$ relative to $proIAPP_{1-22}$ at lower pH is due to the additional electrostatic interaction with the charged histidine, rather than nonelectrostatic interactions involving the histidine side chain.

$ProIAPP_{1-12}$ is a smaller peptide that lacks the disulfide bridge and Arg-22, but contains the tribasic sequence at the cleavage site. At pH 7.4 (±0.3), $proIAPP_{1-12}$ elutes at a conductivity value which is considerably less than that observed for the longer oxidized $proIAPP_{1-22}$ fragment but is close to the value observed for the reduced $proIAPP_{1-22}$ peptide (Figure 4). As expected, the affinity of the peptide varies with net charge, and binding is stronger at low pH (Supporting Information). Although the three basic residues at positions 10−12 are sufficient to confer binding, the removal of the disulfide bridge and C-terminal 10 residues reduces binding significantly. This implies an important role for the disulfide and Arg-22 in HSPG binding. The oxidized $hIAPP_{12-22}$ peptide fragment was also analyzed. This peptide eluted in the void volume at both pH 5.5 (±0.3) and pH 7.4 (±0.3). This demonstrates that the sequence encompassing Lys-22 and Arg-22 is not sufficient to lead to binding in the absence of the basic amino acids at positions 10 and 11. Of the fragments studied, $proIAPP_{1-12}$ contains the minimal residues necessary, i.e., Lys_{10}-Arg_{11}-Lys_{12}, to confer binding to heparin.

Heparan Binding Is Not Due to Amyloid Formation. It is necessary to determine whether these N-terminal proIAPP peptides form amyloid in order to test if aggregation contributes to heparin binding. This is important because it is thought that HSPG binding by mature IAPP is due to aggregation (*28*, *35*). Prior work has demonstrated that

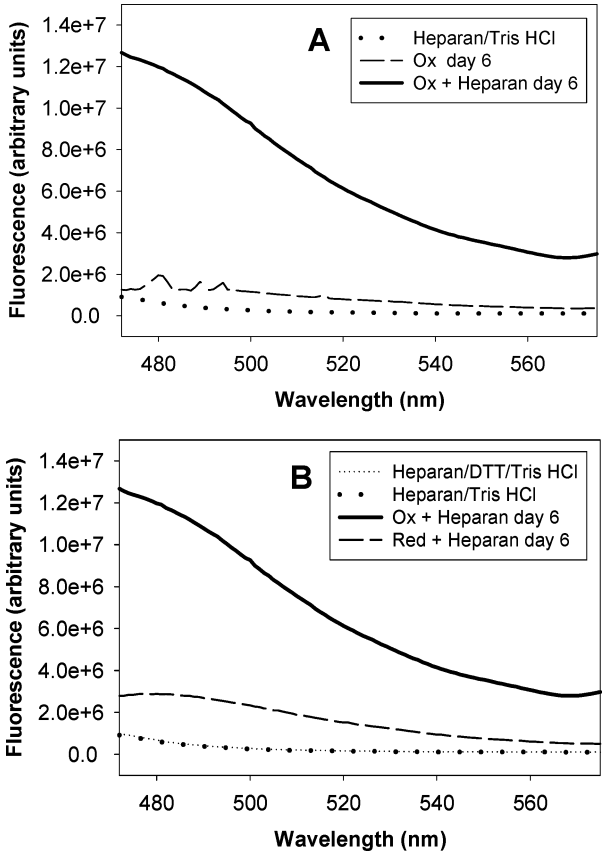

FIGURE 5: Thioflavin-T binding fluorescence of $proIAPP_{1-30}$ at pH 7.4 (±0.3). (A) Oxidized $proIAPP_{1-30}$ (Ox) incubated with (solid lines) and without (dashed lines) heparan sulfate. (B) Oxidized (solid lines) and reduced (Red) (dashed lines) $proIAPP_{1-30}$ incubated with heparan sulfate. Spectra were taken after 6 days of incubation at 1.4 mM peptide concentration and 25 °C. Samples were diluted immediately before recording the emission spectra since the 1.4 mM stock solution is too concentrated for fluorescence measurements. The final peptide concentration was 70.7 μM after dilution.

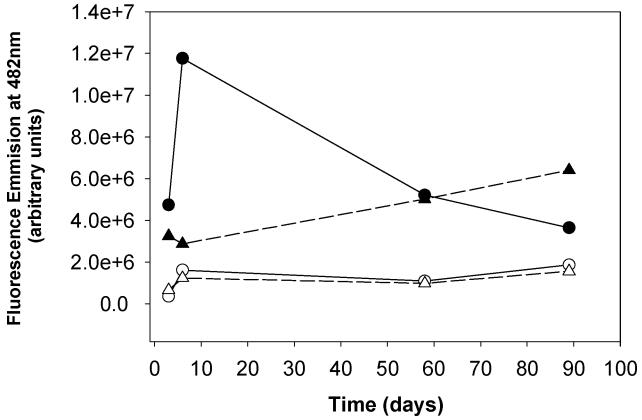

FIGURE 6: Thioflavin-T fluorescence intensity of $proIAPP_{1-30}$ at pH 7.4 (±0.3) plotted as a function of time. Oxidized (●) and reduced (▲) $proIAPP_{1-30}$ incubated with heparan sulfate. Oxidized (○) and reduced (△) $proIAPP_{1-30}$ incubated without heparan sulfate. Spectra were taken after 3, 6, 59, and 89 days of incubation at 1.4 mM peptide concentration and 25 °C. Samples were diluted immediately before recording the emission spectra since the 1.4 mM stock solution is too concentrated for fluorescence measurements. The final peptide concentration was 70.7 μM after dilution. The lines are included as a visual aid and have no theoretical significance.

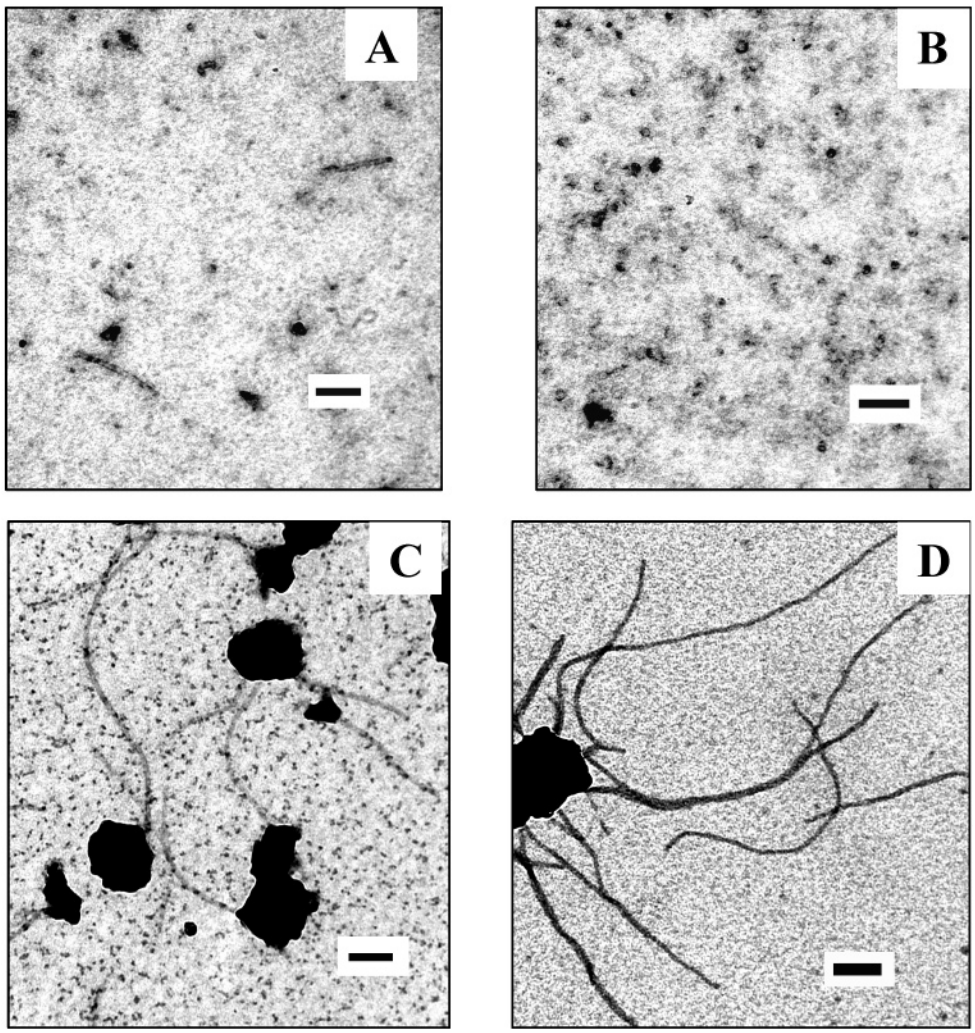

FIGURE 7: TEM images of 1.4 mM proIAPP$_{1-30}$ incubated for 6 days at pH 7.4 (±0.3). (A) Oxidized proIAPP$_{1-30}$. (B) Reduced proIAPP$_{1-30}$. (C) Oxidized proIAPP$_{1-30}$ incubated with heparan sulfate. (D) Reduced proIAPP$_{1-30}$ incubated with heparan sulfate. Scale bars represent 100 nm.

N-terminal and C-terminal cleavage regions of proIAPP are very soluble, unstructured in solution, and do not form amyloid fibrils (*38*). It has been suggested that the first seven residues at the N-terminus of mature IAPP are not amyloidogenic, most likely due to steric constraints imposed on the peptide backbone by the disulfide bridge. The disulfide bridge is believed not to be part of the structured amyloid core of IAPP (*39*−*41*), although it is conserved in all species and is necessary for biological activity of IAPP (*41*). Park and Verchere have previously shown that proIAPP$_{1-30}$ does not form amyloid (*36*). Taken together, these past studies strongly suggest that the N-terminal proIAPP-derived peptides studied here should not form amyloid. Nevertheless, it is important to directly test the ability of our fragments to form amyloid as a control.

Thioflavin-T binding studies show that both the oxidized and reduced forms of proIAPP$_{1-30}$ do not form amyloid even after 6 days of incubation (Figures 5 and 6). These results were confirmed by TEM (Figure 7). In addition, we also tested oxidized and reduced proIAPP$_{1-22}$ by TEM. Samples (5 mM) were prepared in deionized water at pH 7.4 (±0.3), and TEM images were recorded. No amyloid fibrils were detected. These experiments demonstrate that the heparin/heparan sulfate affinity for these N-terminal proIAPP peptides is not due to amyloid formation since the binding studies were preformed immediately after preparing the peptide solutions.

Interaction with Heparan Sulfate Promotes Fibril Formation. We tested the ability of heparan sulfate to enhance amyloid formation at extracellular pH. Incubation of proIAPP$_{1-30}$ with heparan sulfate had a dramatic effect, leading to amyloid formation. Thioflavin-T binding studies of ox-proIAPP$_{1-30}$/HSPG displayed the characteristic increase in fluorescence around 482 nm that is associated with amyloid formation (Figure 5). In contrast, no detectable fluorescence signal in this region was observed for either heparan sulfate alone or peptide alone. The thioflavin-T fluorescence intensity of the ox-proIAPP$_{1-30}$/HSPG sample first increased with time and then gradually decreased. The fluorescence intensity after 6 days was smaller for the red-proIAPP$_{1-30}$/HSPG sample but continued to grow with time (Figure 6). After 58 days the fluorescence signal was the same for both the reduced and oxidized samples incubated with heparan sulfate. At even longer incubation times the signal from the red-proIAPP$_{1-30}$/HSPG sample was larger than the signal from the ox-proIAPP$_{1-30}$/HSPG sample. In contrast, incubation of ox-proIAPP$_{1-30}$ or red-proIAPP$_{1-30}$, in the absence of HSPG, did not lead to any significant gain in thioflavin-T binding even after 89 days of incubation (Figure 6). TEM studies are consistent with the thioflavin-T

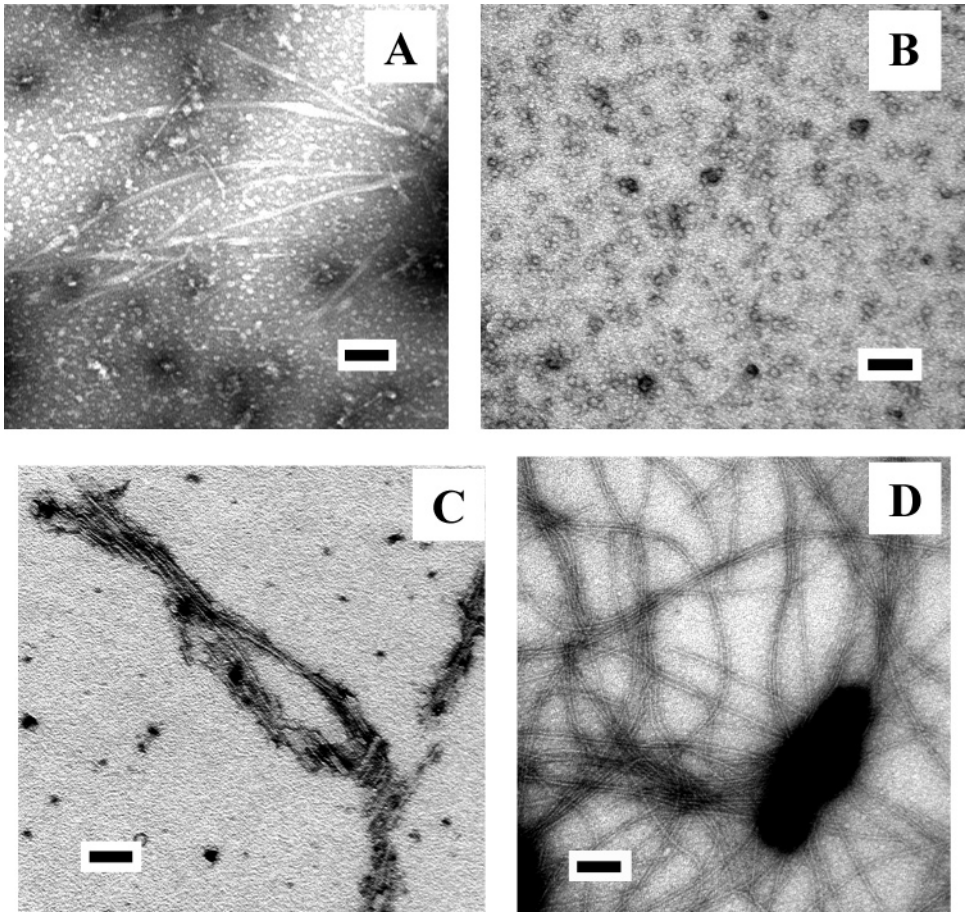

FIGURE 8: TEM of 1.4 mM proIAPP$_{1-30}$ incubated for 89 days at pH 7.4 (±0.3). (A) Oxidized proIAPP$_{1-30}$. (B) Reduced proIAPP$_{1-30}$. (C) Oxidized proIAPP$_{1-30}$ incubated with heparan sulfate. (D) Reduced proIAPP$_{1-30}$ incubated with heparan sulfate. Scale bars represent 100 nm.

binding experiments. Measurements were made with the stock solutions employed for the thioflavin-T binding studies in order to allow direct comparison (see Experimental Procedures). In the presence of heparan sulfate, fibrils were observed for both the reduced and oxidized peptides. After 6 days of incubation, long and narrow fibrils were observed for ox-proIAPP$_{1-30}$/HSPG (Figure 7C and Supporting Information). The fibrils, although not plentiful, have the appearance of amyloid. The fibrils appear to originate from particles of densely stained amorphous material. TEM images of samples containing only heparan sulfate show the same heavily stained particles, indicating that the deposits are heparan sulfate (Supporting Information). These deposits were not observed in samples lacking heparan sulfate. Sparse fibrils were also observed for red-proIAPP$_{1-30}$/HSPG after 6 days of incubation. Again, the fibrils seem to originate from the densely stained heparan sulfate. In stark contrast, the peptide samples incubated in the absence of heparan sulfate did not display any evidence of fibril formation after 6 days. These observations highlight the role of heparan binding in amyloid formation by both oxidized and reduced proIAPP$_{1-30}$. Interestingly, while significantly more fibrils were observed for ox-proIAPP$_{1-30}$/HSPG than red-proIAPP$_{1-30}$/HSPG after 6 days of incubation, the situation was dramatically different after 89 days. A very large number of fibrils were detected for red-proIAPP$_{1-30}$/HSPG, while ox-proIAPP$_{1-30}$/HSPG displayed a more modest amount of fibrils (Figure 8). Furthermore, the fibrils observed for ox-proIAPP$_{1-30}$/HSPG appeared to be shorter and more laterally associated than those observed at the earlier time point. The red-proIAPP$_{1-30}$ sample in the absence of HSPG failed to form fibrils even after 89 days at extracellular pH. Small spherical aggregates were observed. The ox-proIAPP$_{1-30}$ sample, however, showed evidence for small prefibrillar aggregates after 89 days under the same conditions (Figure 8).

Interestingly, the interaction of oxidized proIAPP$_{1-30}$ with heparan sulfate led to a detectable change in the peptide CD spectrum. The spectrum of peptide alone is consistent with a predominantly unstructured ensemble of conformations. In contrast, the CD signal indicates induction of apparent helical structure in the presence of heparan sulfate (Figure 9). However, the CD spectra of amyloid fibrils and prefibrillar aggregates are not well understood and can be difficult to interpret. The important point is that the CD studies provide additional evidence for stronger interactions between HSPG and oxidized peptide compared to HSPG interactions with the reduced peptide. We note that helical precursors have been proposed to play a role in amyloid formation by the Aβ peptide (*42*).

Interactions with heparan sulfate also induced amyloid formation in concentrated samples of proIAPP$_{1-22}$. Sparse fibrils were visualized by TEM within 24 h of sample preparation at pH 7.4 (±0.3). Initially, there were no significant differences in the quantity or morphology of the fibrils detected in the presence of heparan sulfate compared to those observed in the absence of heparan sulfate. After 9 days of incubation, however, an abundance of fibrillar

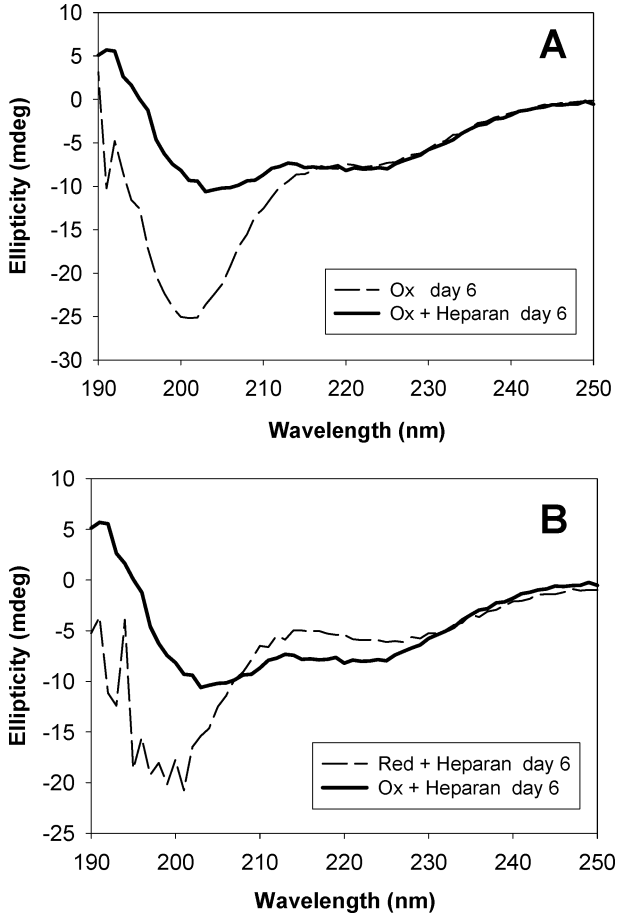

FIGURE 9: Far-UV CD spectra of proIAPP$_{1-30}$ at pH 7.4 (±0.3). (A) Oxidized proIAPP$_{1-30}$ (Ox) incubated with (solid lines) and without (dashed lines) heparan sulfate. (B) Oxidized (solid lines) and reduced (Red) (dashed lines) proIAPP$_{1-30}$ incubated with heparan sulfate. Spectra were taken after 6 days of incubation at 1.4 mM peptide concentration and 25 °C. Samples were diluted immediately before recording the spectra since the peptide stock solutions were too concentrated for CD measurement. The final peptide concentration after dilution was 70.7 μM.

aggregates was present for the sample which contained heparan, but no change was observed for the sample that contained just peptide (Supporting Information). Similar results were obtained for reduced proIAPP$_{1-22}$.

CONCLUSIONS

The biophysical studies described in the previous sections demonstrate several important points. First, incubation with heparan sulfate enhances fibril formation by both proIAPP$_{1-22}$ and proIAPP$_{1-30}$. This provides the first direct evidence that interactions with HSPGs can induce amyloid formation in incorrectly processed IAPP and demonstrates a potential role for HSPGs in IAPP amyloidosis. Second, we find that the disulfide bridge plays a key role in HSPG binding. This may be because the disulfide linkage between Cys-13 to Cys-18 creates a turn or bend that brings His-18, Arg-22, and His-29 in closer proximity to Lys$_{10}$-Arg$_{11}$-Lys$_{12}$ and enhances heparin affinity. There are no structural data for monomeric IAPP; thus it is impossible to determine the conformational consequences of reducing the disulfide. However, IAPP is somewhat similar to human calcitonin gene-related peptide (CGRP) for which a NMR structure is available (*43*). The N-terminal region of human CGRP and IAPP contains a disulfide bridge at identical positions. Structural studies of CGRP indicate the presence of an ordered loop in this region (*43*). Third, comparison of proIAPP$_{1-22}$ and proIAPP$_{1-30}$ shows that His-29 contributes to binding when it is protonated (pH 5.5) but does not make a significant contribution when it is deprotonated (pH 7.4). Sequence analysis of suggested heparin binding sites in amyloid-forming peptides, namely, Aβ, serum amyloid A, prion protein, and β-2-microglobulin, has identified a higher histidine content relative to heparin binding sites in nonamyloidogenic proteins (*27*). Our experiments demonstrate a significant correlation between histidine protonation and heparin affinity for all of the proIAPP fragments studied that contain histidine. It has been proposed that the HSPG perlecan may acidify the local microenvironment of the basement membrane because it is a rather acidic heteropolysaccharide (*27*). If so, this might promote protonation of the histidines and the N-terminus. In addition, HSPG synthesis in type 2 diabetes is believed to be elevated due to increased levels of perlecan mRNA (*44*). Thus, the effects of HSPG's on the charge states of the peptides might be significant. Fourth, both the proIAPP$_{1-22}$ and proIAPP$_{1-30}$ peptides bind heparin considerably more tightly than the proIAPP$_{1-12}$ peptide at both pH 7.4 (±0.3) and pH 5.5 (±0.3). This indicates that while the tribasic sequence at the prohormone convertase cleavage site is necessary for strong binding, it is not sufficient, at least under these conditions.

The TEM and thioflavin-T binding studies of the oxidized and reduced proIAPP$_{1-30}$ peptide in the presence of heparan sulfate reveal several interesting features. These experiments show that while red-proIAPP$_{1-30}$/HSPG is slower to form fibrils, it ultimately forms more extensive fibril deposits. The TEM micrographs also reveal clear differences in the final morphology of the fibrils formed by the oxidized and reduced peptides in the presence of heparan sulfate. The Cys-13 to Cys-18 disulfide forces that region of the polypeptide chain to adopt conformations that are incompatible with the β-sheet structure required in the cross-β motif of an amyloid fibril. Thus, the more extensive fibrils ultimately observed for red-proIAPP$_{1-30}$/HSPG may reflect the fact that a greater fraction of the peptide chain can participate in the amyloid fibril, which in turn could lead to better packing and more stable fibrils. Interestingly, the decrease in thioflavin-T fluorescence for ox-proIAPP$_{1-30}$/HSPG after 6 days of incubation correlates well with the clear morphological differences observed at 6 days and at 89 days in TEM micrographs (Figures 7 and 8). The rodlike fibrils that were present after 6 days of incubation appear to have fragmented by 89 days and laterally associated into thick clumps of short fibrillar structures with frayed ends. One mechanistic scenario that can rationalize these observations is that fibril formation is initially faster for ox-proIAPP$_{1-30}$/HSPG because the peptide is better able to interact with heparan sulfate. The resulting fibrils are, however, less stable because the Cys-13 to Cys-18 disulfide prevents extensive interstrand interactions. As the fibrils elongate, they become unstable and fragment. The resulting fragments then laterally associate, leading to the aggregates observed by TEM at the end of the time course. In contrast, reduced proIAPP$_{1-30}$ interacts more weakly with heparan sulfate, and initial amyloid formation is thus slower. However, the absence of the disulfide allows for more extensive interstrand interactions leading to more stable and

ultimately longer fibrils. Irrespective of the mechanistic details, it is clear that interactions with heparan sulfate enhance fibril formation by both oxidized and reduced proIAPP$_{1-30}$.

The N-terminus of IAPP has been typically overlooked in studies of the mechanism of amyloid formation by IAPP because it is believed not to contribute to the core structure of amyloid (*41*). With recent reports that the proIAPP N-terminal flanking region is uncleaved in a fraction of excreted IAPP in type 2 diabetes, it is important to reevaluate the role of this region in amyloidogenesis. Our studies build upon the important earlier studies of Park and Verchere and have demonstrated that fragments corresponding to the first 22 and first 30 residues of proIAPP are largely nonamyloidogenic in isolation but are capable of forming amyloid fibrils upon interaction with heparan sulfate. These observations indicate that heparan sulfate binding could promote amyloid formation by partially processed proIAPP. This in turn might act as a seed for further amyloid deposition by both IAPP and proIAPP.

Recent investigations have demonstrated that polypeptide−heparin/heparan sulfate interactions are fundamental to amyloidosis and thus are potential drug targets (*45*). For example, a 27-mer peptide fragment modeled after the heparin binding site in serum amyloid A polypeptide (SAA) was evaluated and found to effectively block the interaction of the full-length SAA with HSPGs (*45*). Accumulating evidence indicates the HSPGs may serve as scaffolds, providing an initiation site for amyloid accumulation, and may modulate cytotoxicity by mediating the interaction of amyloid with the cell membrane. The studies reported here should be valuable for designing potential inhibitors of the HSPG/proIAPP interaction.

ACKNOWLEDGMENT

We thank Ms. Susan C. Van Horn for expert assistance with TEM and Ms. Ruchi Gupta for helping to collect some of the TEM images.

SUPPORTING INFORMATION AVAILABLE

Plot of conductivity versus absorbance showing the elution profiles for proIAPP$_{1-12}$ from the heparin-affinity column at pH 3.4 (±0.3), 5.5 (±0.3), and 7.4 (±0.3), TEM micrographs of oxidized proIAPP$_{1-22}$ in the presence and absence of heparan sulfate at pH 7.4 (±0.3), and TEM micrograph of a sample of heparan sulfate collected in the absence of peptide. This material is available free of charge via the Internet at http://pubs.acs.org.

REFERENCES

1. King, H., Aubert, R. E., and Herman, W. H. (1998) Global burden of diabetes, 1995−2025: prevalence, numerical estimates, and projections, *Diabetes Care 21*, 1414−1431.
2. Zimmet, P., Alberti, K. G., and Shaw J. (2001) Global and societal implications of the diabetes epidemic, *Nature 414*, 782−787.
3. Kahn, S. E., D'Alessio, D. A., Schwartz, M. W., Fujimoto, W. Y., Ensinck, J. W., Taborsky, G. J., and Porte, D. (1990) Evidence of cosecretion of islet amyloid polypeptide and insulin by beta-cells, *Diabetes 39*, 634−638.
4. Westermark, P., Wernstedt, C., Wilander, E., Hayden, D. W., O'Brien, T. D., and Johnson, K. H. (1987) Amyloid fibrils in human insulinoma and islets of Langerhans of the diabetic cat are derived from a neuropeptide-like protein also present in normal islet cells, *Proc. Natl. Acad. Sci. U.S.A. 84*, 3881−3885.
5. Cooper, G. J. S., Willis, A. C., Clark, A., Turner, R. C., Sim, R. B., and Reid, K. B. M. (1987) Purification and characterization of a peptide from amyloid-rich pancreases of type 2 diabetic patients, *Proc. Nat. Acad. Sci. U.S.A. 84*, 8628−8632.
6. Clark, A., Lewis, C. E., Willis, A. C., Cooper, G. J. S., Morris, J. F., Reid, K. B. M., and Turner, R. C. (1987) Islet amyloid formed from diabetes-associated peptide may be pathogenic in type-2 diabetes, *Lancet 2*, 231−234.
7. Rushing, P. A., Hagan, M. M., Seeley, R. J., Lutz, T. A., D'Alessio, D. A., Air, E. L., and Woods, S. C. (2001) Inhibition of central amylin signaling increases food intake and body adiposity in rats, *Endocrinology 142*, 5035−5038.
8. Clementi, G., Caruso, A., Cutuli, V. M. C., de bernardis, E., Prato, A., and Amico-Roxas, M. (1996) Amylin given by central or peripheral routes decreases gastric emptying and intestinal transit in the rat, *Experientia 52*, 677−679.
9. Leighton, B., and Cooper G. J. S. (1988) Pancreatic amylin and calcitonin gene-related peptide cause resistance to insulin in skeletal-muscle *in vitro*, *Nature 335*, 632−635.
10. Ohsawa, H., Kanatsuka, A., Yamaguchi, T., Makino, H., and Yoshida, S. (1989) Islet amyloid polypeptide inhibits glucose-stimulated insulin secretion from isolated rat pancreatic islets, *Biochem. Biophys. Res. Commun. 160*, 961−967.
11. Akesson, B., Panagiotidis, G., Westermark, P., and Lundquist, I. (2003) Islet amyloid polypeptide inhibits glucagon release and exerts a dual action on insulin release from isolated islets, *Regul. Pept. 111*, 55−60.
12. Clark, A., Wells, C. A., Buley, I. D., Cruickshank, J. K., Vanhegan, R. I., Matthews, D. R., Cooper, G. J. S., Holman, R. R., and Turner, R. C. (1988) Islet amyloid, increased α-cells, reduced β-cells and exocrine fibrosis: quantitative changes in the pancreas in type 2 diabetes, *Diabetes Res. Clin. Pract. 9*, 151−159.
13. Rocken, C., Linke, R. P., and Saeger, W. (1992) Immunohistology of islet amyloid polypeptide in diabetes mellitus: semiquantitative studies in a post-mortem series, *Virchows Arch. A: Pathol. Anat. Histopathol. 421*, 339−344.
14. Kahn, S. E., Andrikopoulos, S., and Verchere, C. B. (1999) Islet amyloid: a long recognized but underappreciated pathological feature of type 2 diabetes, *Diabetes 48*, 241−246.
15. Butler, A. E., Janson, J., Bonner-Weir, S., Ritzel, R., Rizza, R. A., and Butler, P. C. (2003) β-cell deficit and increased β-cell apoptosis in humans with type 2 diabetes, *Diabetes 52*, 102−110.
16. Hull, R. L., Westermark, G. T., Westermark, P., and Kahn, S. E. (2004) Islet amyloid: a critical entity in the pathogenesis of type 2 diabetes, *J. Clin. Endocrinol. Metab. 89*, 3629−3643.
17. Sanke, T., Bell, G. I., Sample, C., Rubenstein, A. H., and Steiner, D. F. (1988) An islet amyloid peptide is derived from an 89-amino acid precursor by proteolytic processing, *J. Biol. Chem. 263*, 17243−17246.
18. Marcinkiewicz, M., Ramla, D., Seidah, N. G., and Chretien, M. (1994) Developmental expression of the prohormone convertases PC1 and PC2 in mouse pancreatic islets, *Endocrinology 135*, 1651−1660.
19. Marzban, L., Trigo-Gonzalez, G., Zhu, X., Rhodes, C. J., Halban, P. A., Steiner, D. F., and Verchere, C. B. (2004) Role of β-cell prohormone convertase PC (1/3) in processing of pro-islet amyloid polypeptide, *Diabetes 53*, 141−148.
20. Wang, J., Xu, J., Finnerty, J., Furuta, M., Steiner, D. F., and Verchere, C. B. (2001) The prohormone convertase enzyme 2 (PC2) is essential for processing proislet amyloid polypeptide at the NH_2-terminal cleavage site, *Diabetes 50*, 534−539.
21. Furuta, M., Yano, H., Zhou, A., Rouille, Y., Holst, J. J., Carroll, R., Ravazzola, M., Orci, L., Furuta, H., and Steiner, D. F. (1997) Defective prohormone processing and altered pancreatic islet morphology in mice lacking active SPC2, *Proc. Natl. Acad. Sci. U.S.A. 94*, 6646−6651.
22. Westermark, G. T., Steiner, D. F., Gebre-Medhin, S., Engstrom, U., and Westermark, P. (2000) Proislet amyloid polypeptide immunoreactivity in the islets of Langerhans, *Upsala J. Med. Sci. 105*, 97−106.
23. Westermark, P., Engström, U., Westermark, G. T., Johnson, K. H., Permerth, J., and Betsholtz, C. (1989) Islet amyloid polypeptide (IAPP) and pro-IAPP immunoreactivity in human islets of Langerhans, *Diabetes Res. Clin. Pract. 7*, 219−226.
24. Paulsson, J. F., and Westermark, G. T. (2005) Aberrant processing of human proislet amyloid polypeptide results in increased amyloid formation, *Diabetes 54*, 2117−2125.

25. Potter-Perigo, S., Hull, R. L., Tsoi, C., Braun, K. R., Andrikopoulos, S., Teague, J., Verchere, C. B., Kahn, S. E., and Wright, T. N. (2003) Proteoglycans synthesized and secreted by pancreatic islet β-cells bind amylin, *Arch. Biochem. Biophys. 413*, 182−190.
26. Young, I. D., Ailles, L., Narindrasorasak, S., Tan, R., and Kisilevsky, R. (1992) Localization of the basement membrane heparan sulfate proteoglycans in islet amyloid deposits in type 2 diabetes mellitus, *Arch. Pathol. Lab. Med. 116*, 951−954.
27. Ancsin, J. B. (2003) Amyloidogenesis: historical and modern observations point to heparan sulfate proteoglycans as a major culprit, *Amyloid: J. Protein Folding Disord. 10*, 67−79.
28. Castillo, G. M., Cummings, J., Yang, W., Judge, M. E., Sheardown, M. J., Rimvall, K., Hansen, J. B., and Snow, A. D. (1998) Sulfate content and specific glycosaminoglycan backbone of perlecan are critical for perlecan's enhancement of islet amyloid polypeptide (amylin) fibril formation, *Diabetes 47*, 612−620.
29. Inoue, S. (2001) Basement membrane and β amyloid fibrillogenesis in Alzheimer's disease, *Int. Rev. Cytol. 210*, 121−161.
30. Snow, A. D., and Wight, T. N. (1989) Proteoglycans in the pathogenesis of Alzheimer's disease and other amyloidosis, *Neurobiol. Aging 10*, 481−497.
31. Castillo, G. M., Ngo, C., Cummings, J., Wight, T. N., and Snow, A. D. (1997) Perlecan binds to the β-amyloid proteins (Aβ) of Alzheimer's disease, accelerates Aβ fibril formation, and maintains Aβ fibril stability, *J. Neurochem. 69*, 2452−2465.
32. Yamamoto, S., Yamaguchi, I., Hasegawa, K., Tsutsumi, S., Goto, Y., Gejyo, F., and Naiki, H. (2004) Glycosaminoglycans enhance the trifluoroethanol-induced extension of β_2-microglobulin-related amyloid fibrils at a neutral pH, *J. Am. Soc. Nephrol. 15*, 126−133.
33. Suk, J. Y., Zhang, F., Balch, W. E., Linhardt, R. J., and Kelly, J. W. (2006) Heparin accelerates gelsolin amyloidogenesis, *Biochemistry 45*, 2234−2242.
34. Mulloy, B., and Forster, M. J. (2000) Conformation and dynamics of heparin and heparan sulfate, *Glycobiology 10*, 1147−1156.
35. Watson, D. J., Lander, A. D., and Selkoe, D. J. (1997) Heparin-binding properties of the amyloidogenic peptides Aβ and amylin. Dependence on aggregation state and inhibition by Congo Red, *J. Biol. Chem. 272*, 31617−31624.
36. Park, K., and Verchere, C. B. (2001) Identification of a heparin binding domain in the N-terminal cleavage site of pro-islet amyloid polypeptide. Implications for islet amyloid formation, *J. Biol. Chem. 276*, 16611−16616.
37. Abedini, A., Singh, G., and Raleigh, D. P. (2006) Recovery and purification of highly aggregation prone disulfide containing peptides: Application to islet amyloid polypeptide, *Anal. Biochem. 351*, 181−186.
38. Nilsson, M. (2000) Amyloid formation by amylin, Ph.D. Dissertation, State University of New York at Stony Brook, Stony Brook, NY.
39. Sunde, M., Serpell, L. C., Bartlam, M., Fraser, P. E., Pepys, M. B., and Blake, C. C. F. (1997) Common core structure of amyloid fibrils by synchrotron X-ray diffraction, *J. Mol. Biol. 273*, 729−739.
40. Goldsbury, C., Goldie, K., Pellaud, J., Seelig, J., Frey, P., Muller, S. A., Kistler, J., Cooper, G. J. S., and Aebi, U. (2000) Amyloid fibril formation from full-length and fragments of Amylin, *J. Struct. Biol. 130*, 352−362.
41. Jaikaran, E. T. A. S., Higham, C. E., Serpell, L. C., Zurdo, J., Gross, M., Clark, A., and Fraser, P. E. (2001) Identification of a novel human islet amyloid polypeptide β-sheet domain and factors influencing fibrillogenesis, *J. Mol. Biol. 308*, 515−525.
42. Kirkitadze, M. D., Condron, M. M., and Teplow, D. B. (2001) Identification and characterization of key kinetic intermediates in amyloid β-protein fibrillogenesis, *J. Mol. Biol. 312*, 1103−1119.
43. Breeze, A. L., Harvey, T. S., Bazzo, R., and Campbell, I. D. (1991) Solution structure of human calcitonin gene-related peptide by ^{1}H-NMR and distance geometry with restrained molecular dynamics, *Biochemistry 30*, 575−582.
44. Conde-Knape, K. (2001) Heparan sulfate proteoglycans in experimental model of diabetes: a role for perlecan in diabetes complications, *Diabetes Metab. Res. Rev. 17*, 412−421.
45. Elimova, E., Kisilevsky, R., Szarek, W. A., and Ancsin, J. B. (2004) Amyloidogenesis recapitulated in cell culture: a peptide inhibitor provides direct evidence for the role of heparan sulfate and suggests a new treatment strategy, *FASEB J. 18*, 1749−1751.

BI0510936